PRAMANA
—journal of
physics

© Printed in India

Vol. 50, No. 2,
February 1998
pp. 173–189

Measurement and analysis of the excitation function and isomeric cross section ratios for α-induced reaction on Ir, Au, Re and Ta nuclei

M ISMAIL
Variable Energy Cyclotron Centre, I/AF, Bidhan Nagar, Calcutta 700 064, India
Email: ismail@veccal.ernet.in

MS received 3 December 1996; revised 18 June 1997

Abstract. Excitation functions and a few isomeric cross-section ratios for production of (1) ^{192}Au, ^{193}Au, ^{194}Au, ^{195}Au and ^{192}Ir nuclides in α-induced reactions on ^{191,193}Ir, (2) ^{197}Tl, ^{197m}Hg, ^{198m,g}Tl, ^{199}Tl and ^{200}Tl nuclides in α-induced reaction in ^{197}Au and (3) ^{183}Re and ^{184m,g}Re nuclides in α-induced reaction in ^{181}Ta and ^{185}Re are obtained from the measurements of the residual activities by the conventional stacked-foils technique from threshold to 50 MeV. The excitation function and isomeric cross-section ratios for nuclear reaction ^{181}Ta$(\alpha, n)^{184m,g}$Re are compared with the theoretical calculation using the code Stapre which is based on exciton model for pre-equilibrium phase and Hauser–Feshbach formalism taking angular momentum and parity into account for the equilibrium phase of the nuclear reaction. All other experimental excitation functions are compared with the calculations considering equilibrium as well as pre-equilibrium reaction mechanism according to the geometry dependent hybrid (GDH) model and hybrid model of Blann using the code Alice/91. The high energy part of the excitation functions are dominated by pre-equilibrium reaction mechanism whereas the low energy parts are dominated by equilibrium evaporation with its characteristic peak. The GDH model provides a potentially better description of the physical process (i.e., a higher probability for peripheral collisions to undergo precompound decay than for central collisions) compared to hybrid model. However in the energy range of present measurement most of the excitation functions are fitted reasonably well by both GDH model and hybrid model with initial exciton number $N_0 = 4(N_n = 2, N_p = 2, N_h = 0)$. Barring a few reactions we have found the overall agreement between theory and experiment is reasonably good taking the limitations of the theory into account.

Keywords. α-induced reactions on Ir, Au, Re and Ta; stacked foil technique; isotope production; equilibrium and pre-equilibrium decays; Stapre and Alice/91 codes.

PACS No. 25.60

1. Introduction

It is well known that the compound statistical model coupled with the exciton model gives a correct overall description of the excitation functions and particle energy spectra in nuclear reactions at medium energies. However, the calculations partially fail to account for details such as the exact position of the maximum or the slope of the ascending and descending part of the excitation functions. The high energy parts of the excitation functions are dominated by pre-equilibrium reaction mechanism whereas the low energy parts are dominated by evaporation with its characteristic peak. The pre-equilibrium

processes have been investigated by several authors [1–6]. Excitation functions for equilibrium and pre-equilibrium reactions have been studied in (α, xn) and (α, pxn) reactions [7–10]. Theoretical calculations for pre-equilibrium process have been carried out in terms of exciton models [1–3]. Several models [1–6, 11–15] have been proposed to explain the emission of energetic light particles by the equilibration process from the nuclear system excited at medium energies. Predictions from these models with regard to excitation functions and the energy spectra of the emitted particles compared well with the existing experimental data. This has prompted a continued interest in these models as tools both to predict cross-sections for a number of nuclear reactions for practical purposes and to test the adequacy of the underlying physics. The isomeric cross-section ratios for a pair of isomeric states are known to depend strongly on the spins of the isomers concerned as well as on the spins of the higher lying levels populating the isomers. Experimental and theoretical studies on the isomeric cross-section ratios specially as function of incident particle energy should therefore lead to useful information on the spin cut off parameter as well as on the level structure of the residual nuclei. The excitation functions and isomeric cross-section studies are significant for the investigation of the mechanism of nuclear reactions. The present work on alpha induced reactions on the target nuclei ^{181}Ta, ^{185}Re, ^{191}Ir and ^{193}Ir is also intended to supply some new data in the alpha energy range from threshold to 50.0 MeV. Since the nuclear reactions ^{197}Au$(\alpha, xnypz\alpha)$ have already been studied extensively by several authors (see [16] and references therein), we have measured the cross-sections and the isomeric cross-section ratios for ^{197}Au$(\alpha, xnypz\alpha)$ reactions so as to standarize our measurements by comparing our measurements with previous measurements. Hence the nuclear reactions ^{197}Au$(\alpha, xnypz\alpha)$ have not been given much importance for theoretical analysis. However the nuclear reaction cross-sections are being presented in this paper only for completeness.

This paper continues a series of reports on gross features of the interactions of intermediate energy light projectile with medium and heavy nuclei. The experiments have been performed at the Variable Energy Cyclotron Centre, Calcutta. Several excitation functions for the reactions ^{191,193}Ir(α, xn) $^{195-x,197-x}$Au, ^{191}Ir$(\alpha, \alpha n)$ ^{192}Ir, ^{197}Au(α, xn) $^{200-x}$Tl, ^{197}Au$(\alpha, p3n)$ ^{197}Hg, ^{185}Re$(\alpha, \alpha n)$ ^{184}Re and ^{181}Ta(α, xn) $^{185-x}$Re measured by the stacked foil technique are presented. The excitation functions of the radioactive products observed in reactions contain some information about the mechanism of the interaction of the α-particles with Ir, Ta Re and Au nuclei. In this work calculations in the framework of the equilibrium statistical model and pre-equilibrium model using the code Alice/91 [17] and Stapre [18] were performed and the results are compared with experimental excitation functions. The Stapre code [18] which is based on exciton model for pre-equilibrium phase and Hauser–Feshbach formalism taking angular momentum and parity into account for the equilibrium phase has been used to calculate isomeric cross-section ratios and the results are compared with the measured isomeric cross-section ratios.

2. Experimental procedure

Excitation functions for alpha induced reactions on ^{181}Ta, ^{191}Ir, ^{193}Ir and ^{197}Au were determined using the absolute yields of characteristic γ-rays pertaining to the decay of

each radioactive residual nuclide as usually done in stacked foil technique. The targets were commercially available thin self-supporting foils. The thicknesses of gold foils were 4.837 μm, that of irridium foils 13.021 μm, and tantalum foils were 10.521 μm obtained by weighing. Then the stacks were irradiated in a chamber (as shown in figure 1 of [9]) specially constructed for this purpose having the facility to irradiate up to four stacks one after another. The beam spot on the targets was limited to 5.0 mm in diameter by using a 10.0 cm long aluminum collimator in front of the targets. The Au and Ta stack consisted of about 20 targets whereas Ir stack consisted of about 15 targets. Since the Au foils were very thin, these were interspersed with 23.4 μm thick Al degrader-cum-catcher foils. The stacks were exposed to the unanalysed external beam from the 224 cm variable energy cyclotron in Calcutta. The beam current on the targets was kept below 200 nA. The total α-particle beam was collected and measured using a calibrated ORTEC current integrator. The absolute cross-sections for the reactions ^{197}Au(α, *xnypαz*) were also compared with previous measurements [16]. The cross-section for the α-induced reaction on Au are very well known [16]. Comparison of ^{200}Tl, ^{199}Tl and ^{198}Tl production cross-section from previous measurements with our measurements thus provides high reliability to the absolute cross-section measurements. The unanalysed beam energy resolution was $\simeq$ 0.2 MeV. The accuracy in absolute energy is expected to be $\cong$ 2.0 MeV. However from some of the excitation functions for the α-induced reactions on Au the energies were re-calibrated with respect to their thresholds and thereby improving the accuracy in absolute energy to $\cong$ 0.5 MeV.

The mean beam energy at the half-thickness of each target of a stacked foil assembly was calculated from the energy degradation of the initial beam energy according to the given stopping power values for different materials. We have used the stopping powers from the tabulated values of Williamson *et al* [19]. However the tabulated values are in multiple of 2.0 MeV up to 50.0 MeV and in steps of 5.0 MeV thereafter. Therefore interpolation is required at every foil of the stack. To improve the accuracy of interpolation the stopping powers $S(E)$ are fitted by a non-linear least square method to a function of the form:

$$S(E) = \sum_{i=1,4} A_i \cdot E^{i-1} + \sum_{k=1,2} B_k \cdot \exp(-C_k \cdot E), \tag{1}$$

where A_i, B_k and C_k are the constants to be determined from non-linear least square fit. The fit improves the overall accuracy of the stopping power interpolation. The average thicknesses of the target and degrader foils were determined by weighing. Each foil was cut out into a square shape and pasted over an annular Al ring having 30.0 mm as the outer diameter.

The γ-rays emitted by the activated foils were detected either with a Ge(Li) detector or with a HPGe detector (both having 30% efficiency) available at our centre. In most of the cases the γ-rays, used in yield determination as listed in table 1, stand out very prominently in the spectra and does not pose any identification problem. The γ-ray spectra from the Ge(Li) and HPGe detectors were analysed using personal computer based multi channel analyser and were stored on hard disk or floppy diskettes. The Super-32 computer was used to analyse the γ-ray spectra stored on these hard disk and floppy diskettes. One program EXPANL1 was written to select the required peaks from the γ-ray spectra stored on hard disk and floppy diskettes and prepare a data file EXP2DT. Another program ISABELLE written by Kern [20, 21] (modified and renamed as EXPANL2) was

Table 1. Half-lives, γ-energies, branching ratios of the γ-decays and Q-values for α-induced reactions on Ir, Au, Re and Ta.

Nuclide	Half-lives	E_γ (keV)	I_γ(%)	Reaction	Q-values (MeV)
^{192}Au	4.94 h	316.51	58.00	^{191}Ir(α, 3n)	−25.709
				^{193}Ir(α, 5n)	−39.679
^{193}Au	17.65 h	186.17	10.11	^{191}Ir(α, 2n)	−16.944
				^{193}Ir(α, 4n)	−30.914
^{194}Au	38.02 h	328.50	60.00	^{191}Ir(α, n)	−10.084
				^{193}Ir(α, 3n)	−24.054
^{195}Au	186.09 d	98.88	10.90	^{193}Ir(α, 2n)	−15.670
^{192}Ir	73.83 d	316.51	82.81	^{193}Ir(α, 2p3n)	−36.053
				^{193}Ir(α, αn)	−7.757
				^{191}Ir(α, 2pn)	−22.084
^{197}Tl	2.84 h	425.84	12.91	^{197}Au(α, 4n)	−32.606
		152.23	07.21	^{197}Au(α, 4n)	−32.606
^{197m}Hg	23.80 h	133.96	34.00	^{197}Au(α, p3n)	−29.678
^{198g}Tl	5.30 h	411.80	82.10	^{197}Au(α, 3n)	−25.434
^{198m}Tl	1.87 h	282.80	28.00	^{197}Au(α, 3n)	−25.434
^{199}Tl	7.42 h	455.46	12.31	^{197}Au(α, 2n)	−16.813
		208.21	12.21	^{197}Au(α, 2n)	−16.813
^{200}Tl	26.10 h	367.94	87.20	^{197}Au(α, n)	−09.736
^{183}Re	71.20 d	162.33	23.58	^{181}Ta(α, 2n)	−16.340
^{184g}Re	38.00 d	792.07	37.64	^{181}Ta(α, n)	−09.873
^{184m}Re	169.8 d	252.85	10.89	^{181}Ta(α, n)	−09.873
^{184g}Re	38.00 d	792.07	37.64	^{185}Re(α, 2p3n)	−35.975
^{184m}Re	169.8 d	252.85	10.89	^{185}Re(α, 2p3n)	−35.975
				^{185}Re(α, αn)	−07.679

h = hour, d = days, y = year.

used to analyse the peaks stored in the data file EXP2DT. The program ISABELLE fits the γ-ray spectra very well (see figure 2d in [9]). The integration of the analytical function as well as experimental peak was used for yield determination. The γ-ray yield was determined by integrating the experimental peak points and subtracting the calculated background from it.

The efficiency calibrations of the detector were done with a standard ^{152}Eu and ^{133}Ba radioactive source obtained from B.R.I.T. (Department of Atomic Energy) available at our centre. The efficiency of the detector was interpolated to the required energy value from the measured efficiency curve. However to improve the interpolation, the efficiency curve was similarly fitted by a non-linear least square method to a function of the form given in (1). The range of the fit was from 122 keV to 1408 keV. The fit improves the accuracy of interpolation considerably. For γ-ray having energy $E_\gamma < 122$ keV, the efficiency of the detector was extracted by manually plotted efficiency curve using low energy γ-rays from ^{152}Eu and ^{133}Ba calibrated sources.

The nuclear data necessary for the evaluation of the cross-sections are presented in table 1. The half-lives of the radioactive atoms are taken from the chart of nuclides [22],

the γ-ray energies and branching ratios are taken from the table of isotopes [22]. In table 1, only those γ-rays are listed which were chosen for the calculation of the cross-sections. Also included in table 1 are reaction Q-values. Q-values were calculated using the atomic mass table of Wapstra and Audi [23].

2.1 *Cross-section determination*

The number of observed decays Z per unit time is related to the total number of decays Z_0 per unit time by

$$Z_0 = Z/[\varepsilon(E_\gamma) * I_\gamma(\text{abs})], \tag{2}$$

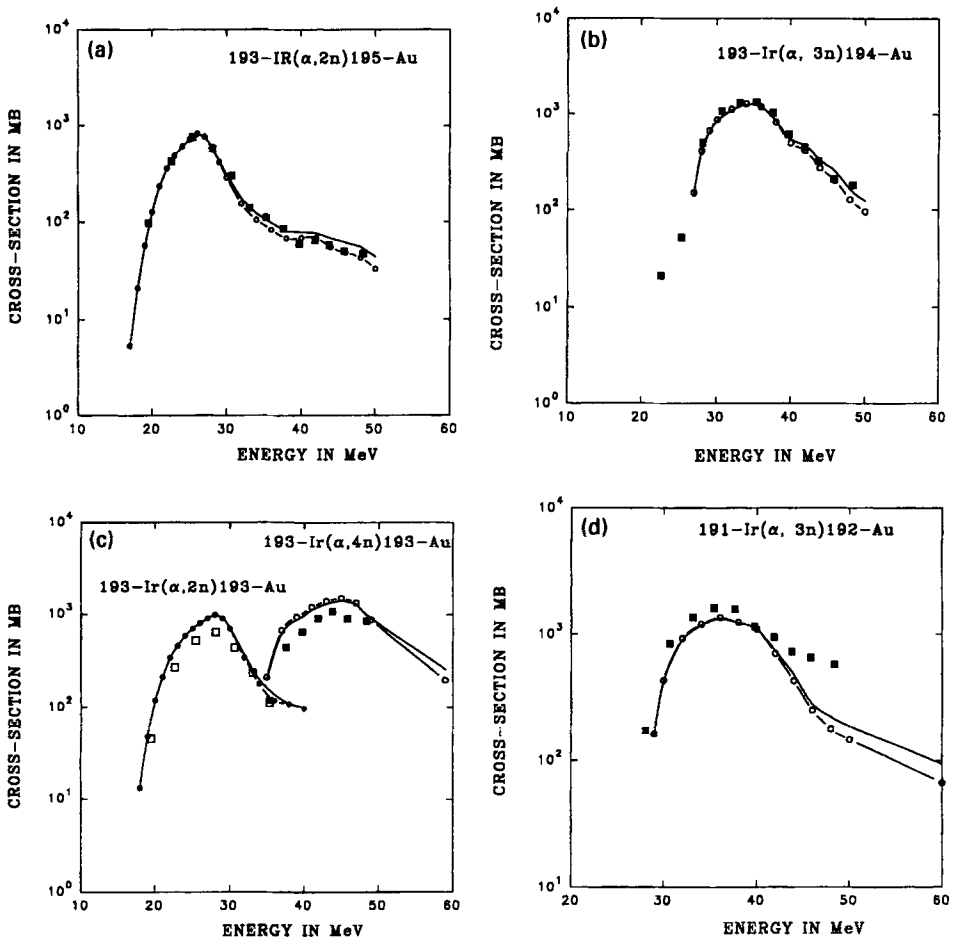

Figure 1a–d. The total residual production cross-section in mb for the reactions **(a)** $^{193}\text{Ir}(\alpha, 2n)^{195}\text{Au}$ (■), **(b)** $^{193}\text{Ir}(\alpha, 3n)^{194}\text{Au}$ (■), **(c)** $^{(193),191}\text{Ir}[\alpha, (4n)\,2n]^{193}\text{Au}$ [(■), □] and **(d)** $^{191}\text{Ir}(\alpha, 3n)^{192}\text{Au}$ (■) are plotted as a function of α-particle bombarding energy. The solid line is the geometry dependent hybrid model and the circle-line (–○–) is the hybrid model fits using the code Alice/91 with $N_0 = 4, N_n = 2, N_p = 2$ and $N_h = 0$.

where $\epsilon(E_\gamma)$ is the detector efficiency and I_γ(abs) is the absolute γ-ray abundance per decay. The total number of decays, Z_0, is related to total reaction yield R for simple decays (simple decays correspond to direct production of radio isotopes by the nuclear reactions and we have used only such decays in all the measurements reported here) by the relation

$$R = Z_0 \cdot \exp(\lambda T_2)/[(1 - \exp(-\lambda T)) \cdot (1 - \exp(-\lambda T_1))/\lambda T_1], \quad (3)$$

where λ is the decay constant, T_1 the irradiation time, T_2 the cooling time after the end of irradiation and the beginning of the measurement, T the counting time and R is related to the cross-section σ by the relation

$$\sigma = R/[(N_A \cdot \delta x) \cdot \mathcal{J}], \quad (4)$$

Table 2. Experimental cross-section for α-induced reaction with ^{191}Ir and ^{193}Ir.

Energy in (MeV)	From ^{191}Ir		
	192-Au ($3n$)	193-Au ($2n$)	194-Au (n)
48.4 ±0.9	580.62 ±0.30%		
45.8 ±1.0	656.41 ±0.70%		
43.8 ±1.0	727.27 ±0.80%		
41.9 ±1.0	939.84 ±0.70%		
39.7 ±1.1	1141.51 ±0.40%		
37.6 ±1.1	1562.89 ±0.30%		
35.4 ±1.1	1602.75 ±0.30%	110.9* ±0.80%	
33.1 ±1.2	1349.15 ±0.40%	236.26 ±1.50%	
30.7 ±1.2	841.48 ±0.60%	438.09 ±2.50%	23.3* ±0.15%
28.1 ±1.3	172.789 ±2.10%	640.60 ±1.40%	29.8* ±0.24%
25.4 ±1.4		522.11 ±0.30%	32.7* ±0.80%
22.6 ±1.5		269.65 ±0.30%	35.6 ±1.60%
19.5 ±1.6		45.74 ±0.70%	33.64 ±1.00%
16.1 ±1.8			3.14 ±1.00%

Table 2. (*Continued*)

Energy in (MeV)	Cross-section of the product in milli barns from ^{193}Ir			
	195-Au ($2n$)	192-Ir (αn)	194-Au ($3n$)	193-Au ($4n$)
48.4 ±0.9	47.06 ±8.20%	196.998 ±0.46%	179.462 ±1.30%	854.336 ±2.00%
45.8 ±1.0	49.72 ±5.27%	83.863 ±0.46%	207.039 ±1.10%	899.380 ±3.00%
43.8 ±1.0	57.23 ±5.30%	52.057 ±1.00%	320.463 ±0.90%	1077.775 ±1.00%
41.9 ±1.0	64.28 ±4.00%	37.069 ±0.69%	445.464 ±0.60%	904.602 ±0.80%
39.7 ±1.1	59.18 ±5.00%	28.935 ±1.50%	608.938 ±0.30%	644.735 ±0.60%
37.6 ±1.1	84.80 ±2.60%	25.356 ±1.70%	1028.389 ±0.16%	441.116 ±0.60%
35.4 ±1.1	110.63 ±2.54%	18.491 ±1.75%	1342.906 ±0.08%	118.3* ±1.80%
33.1 ±1.2	139.56 ±2.07%	11.801 ±3.07%	1318.248 ±0.12%	
30.7 ±1.2	303.44 ±0.96%	6.505 ±6.10%	1061.1 ±0.15%	
28.1 ±1.3	580.44 ±0.52%	4.193 ±9.10%	478.3* ±0.24%	
25.4 ±1.4	757.07 ±0.42%	2.053 ±9.90%	17.0* ±0.80%	
22.6 ±1.5	426.80 ±0.93%	1.686 ±10.0%		
19.5 ±1.6	97.49 ±2.73%	1.686 ±10.0%		

where N_A is the number of atoms/cm^3 of the target material, δx is the thickness of the foil (in cm) and $\mathcal{J}$ is the total number of incident particles during the irradiation (calculated from total charge measured by current integrator).

3. Experimental results

In table 2 and figures (1a) to (1d) our experimental results for the production of ^{192}Au, ^{192}Ir, ^{193}Au, ^{194}Au and ^{195}Au radio-nuclides via α-induced reactions on ^{191,193}Ir are summarized and plotted as a function of α-particle bombarding energy. The experimental cross-sections are in millibarns and presented along with the percentage of statistical errors only. Since the radio-nuclides ^{193}Au could be produced by ^{191}Ir$(\alpha, 2n)$ and ^{193}Ir$(\alpha, 4n)$ reactions and the radio-nuclides ^{194}Au could be produced by ^{191}Ir(α, n) and ^{193}Ir$(\alpha, 3n)$ reactions, in the overlapping regions the cross-sections for these reactions are taken as proportional to their theoretical values based on the GDH model calculation [6].

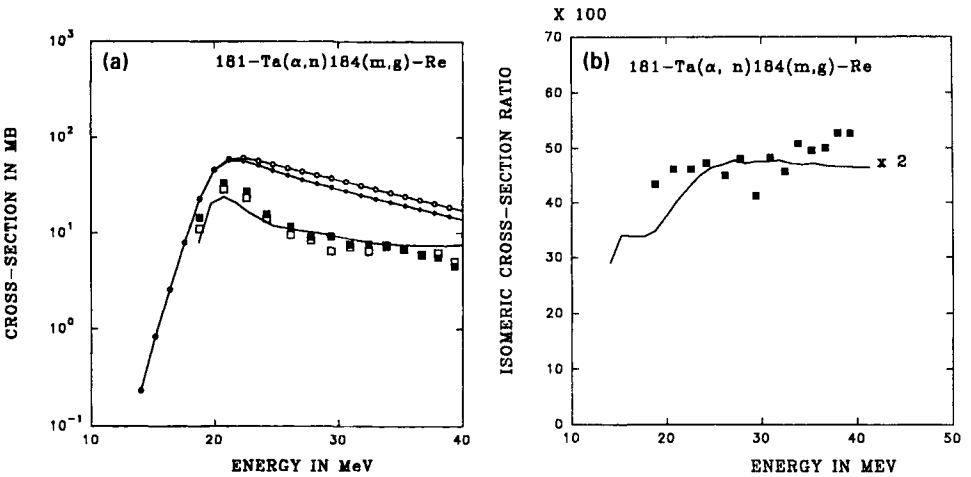

Figure 2. (**a**) The total residual production cross-section in mb for the reaction $^{181}\text{Ta}(\alpha, n)^{184m,g}\text{Re}$ [■ ⇒ g, □ ⇒ m] are plotted as a function of α-particle bombarding energy. The solid line is the geometry dependent hybrid model fit using the code Alice/91 with $N_0 = 4, N_n = 2, N_p = 2$ and $N_h = 0$. The –•– and –o– are Stapre code calculation with $FM = 1000.0\,(\text{MeV})^3$ and $FM = 750\,(\text{MeV})^3$ respectively. (**b**) The isomeric cross-section ratios for the isomer pair $^{184m,g}\text{Re}$ are plotted (■) as a function of α-particle bombarding energy. The solid lined curve is Stapre code calculation with $FM = 1000\,(\text{MeV})^3$. The curve with $FM = 750\,(\text{MeV})^3$ is indistinguishable with the plotted solid curve.

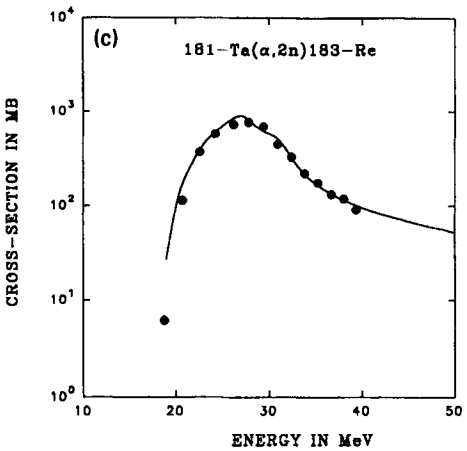

Figure 2c. The total residual production cross-section in mb for the reaction $^{181}\text{Ta}(\alpha, 2n)^{183}\text{Re}$ (•) are plotted as a function of α-particle bombarding energy. The solid line is the geometry dependent hybrid model fit using the code Alice/91 with $N_0 = 4, N_n = 2, N_p = 2$ and $N_h = 0$.

These points are marked with symbols (*) in table 2 and beyond these marked points the contributions of (α, n) and $(\alpha, 2n)$ reactions to $(\alpha, 3n)$ and $(\alpha, 4n)$ reactions respectively are negligible (< 2%). The number of such points for $(\alpha, 2n)$ and $(\alpha, 4n)$ reactions is

Table 3. Experimental cross-section for α-induced reaction with ^{181}Ta.

Energy in (MeV)	Cross-section of the product in milli barns			
	183-Re	184-Re (g)	184-Re (m)	$\sigma_m/(\sigma_g+\sigma_m)$
18.8 ±1.0	6.09 ±1.5%	14.45 ±0.63%	11.07 ±3.0%	0.434
20.7 ±1.0	114.23 ±0.3%	33.50 ±0.69%	28.76 ±2.6%	0.462
22.6 ±0.9	375.89 ±0.09%	27.23 ±0.48%	23.36 ±2.1%	0.462
24.2 ±0.8	581.04 ±0.11%	15.78 ±1.08%	14.17 ±6.3%	0.473
26.2 ±0.8	730.62 ±0.08%	11.62 ±0.11%	9.50 ±7.4%	0.450
27.8 ±0.8	772.58 ±0.05%	9.07 ±0.81%	8.38 ±7.3%	0.480
29.4 ±0.8	698.82 ±0.11%	9.13 ±1.52%	6.41 ±10.0%	0.412
30.9 ±0.8	457.57 ±0.13%	7.54 ±1.69%	7.03 ±9.4%	0.482
32.5 ±0.8	334.07 ±0.15%	7.65 ±1.62%	6.43 ±7.8%	0.457
33.9 ±0.7	224.18 ±0.18%	7.14 ±1.72%	7.36 ±8.7%	0.508
35.3 ±0.7	177.45 ±0.20%	6.87 ±1.73%	6.73 ±7.9%	0.495
36.7 ±0.7	132.90 ±0.24%	5.86 ±1.91%	5.87 ±5.8%	0.500
38.0 ±0.7	118.90 ±0.26%	5.48 ±2.03%	6.11 ±7.3%	0.527
39.3 ±0.7	91.25 ±0.28%	4.47 ±2.20%	4.97 ±9.2%	0.526

Table 4. Experimental cross-section for α-induced reaction with ^{185}Re.

Energy in (MeV)	Cross-section of the product in milli barns		
	184-Re (g)	184-Re (m)	$\sigma_m/(\sigma_g+\sigma_m)$
32.6 ± 2.0	3.83 ± 5.0%	4.07 ± 10.0%	0.515
36.6 ± 2.0	4.29 ± 4.8%	5.28 ± 10.0%	0.552
40.5 ± 2.0	12.11 ± 1.8%	11.67 ± 9.0%	0.491
44.2 ± 1.8	18.33 ± 0.45%	18.73 ± 3.3%	0.505
47.6 ± 1.7	26.15 ± 0.55%	28.00 ± 4.2%	0.517

only one and for (α, n) and $(\alpha, 3n)$ reactions three. Since no data exist in literature for α-induced reactions on ^{191,193}Ir, comparison could not be made with other measurements. In table 3 and figures 2a and 2c the total residual production cross-section in mb for

Table 5. Experimental cross-section for α-induced reaction with ^{197}Au.

Energy in (MeV)	Cross-section of the product in milli barns				
	200-Tl	199-Tl	198-Tl (g)	198-Tl (m)	$\sigma_m/(\sigma_m+\sigma_g)$
52.0 ± 0.3	$1.95 \pm 1.9\%$	$37.29 \pm 3.8\%$	$174.15 \pm 0.3\%$	$254.18 \pm 8.6\%$	0.594
50.7 ± 0.3	$2.16 \pm 1.7\%$	$45.12 \pm 3.0\%$	$211.19 \pm 0.3\%$	$328.57 \pm 7.1\%$	0.608
49.4 ± 0.3	$2.18 \pm 1.7\%$	$44.50 \pm 3.1\%$	$232.51 \pm 0.4\%$	$337.97 \pm 5.9\%$	0.592
48.0 ± 0.3	$2.43 \pm 1.8\%$	$47.79 \pm 2.3\%$	$289.24 \pm 0.2\%$	$433.42 \pm 3.3\%$	0.600
46.6 ± 0.3	$2.52 \pm 1.8\%$	$51.45 \pm 1.6\%$	$364.37 \pm 0.2\%$	$521.26 \pm 2.6\%$	0.589
45.1 ± 0.3	$2.43 \pm 1.7\%$	$48.96 \pm 1.4\%$	$406.23 \pm 0.2\%$	$735.08 \pm 2.7\%$	0.644
43.6 ± 0.3	$2.88 \pm 1.6\%$	$57.17 \pm 0.8\%$	$564.90 \pm 0.18\%$	$990.33 \pm 1.8\%$	0.637
42.1 ± 0.3	$3.08 \pm 1.7\%$	$65.55 \pm 1.2\%$	$750.94 \pm 0.3\%$	$1230.85 \pm 1.4\%$	0.621
40.6 ± 0.3	$3.82 \pm 0.5\%$	$82.25 \pm 0.8\%$	$959.55 \pm 0.2\%$	$1417.20 \pm 1.2\%$	0.596
38.8 ± 0.3	$4.40 \pm 0.6\%$	$101.29 \pm 0.9\%$	$1059.09 \pm 0.2\%$	$1518.60 \pm 1.0\%$	0.589
37.2 ± 0.4	$4.90 \pm 0.6\%$	$129.20 \pm 0.56\%$	$1011.62 \pm 0.2\%$	$1485.62 \pm 1.0\%$	0.595
35.5 ± 0.4	$5.50 \pm 0.6\%$	$184.27 \pm 0.5\%$	$925.02 \pm 0.2\%$	$1266.36 \pm 0.8\%$	0.578
33.7 ± 0.4	$7.49 \pm 0.5\%$	$317.88 \pm 0.3\%$	$783.06 \pm 0.3\%$	$1023.21 \pm 1.3\%$	0.567
31.8 ± 0.4	$7.03 \pm 0.7\%$	$485.13 \pm 0.2\%$	$483.44 \pm 0.4\%$	$612.74 \pm 1.9\%$	0.559
29.9 ± 0.4	$8.28 \pm 0.5\%$	$723.71 \pm 0.16\%$	$196.75 \pm 0.4\%$	$208.55 \pm 0.6\%$	0.515
27.8 ± 0.4	$9.32 \pm 0.2\%$	$710.79 \pm 0.16\%$	$23.65 \pm 2.2\%$	$15.44 \pm 2.0\%$	0.390
26.5 ± 0.4	$9.61 \pm 0.22\%$	$708.60 \pm 0.4\%$			
25.6 ± 0.4	$10.58 \pm 0.4\%$	$649.12 \pm 0.4\%$			
25.6 ± 0.4	$12.53 \pm 0.8\%$	$571.78 \pm 0.2\%$			
24.8 ± 0.5	$12.10 \pm 0.2\%$	$554.83 \pm 0.5\%$			
24.0 ± 0.5	$15.19 \pm 0.4\%$	$500.91 \pm 0.4\%$			
23.3 ± 0.5	$16.86 \pm 0.5\%$	$345.53 \pm 0.33\%$			
23.1 ± 0.5	$19.90 \pm 0.9\%$	$362.57 \pm 1.0\%$			
22.2 ± 0.5	$22.32 \pm 0.2\%$	$282.92 \pm 0.9\%$			
21.0 ± 0.5	$26.88 \pm 0.8\%$	$173.76 \pm 0.86\%$			
20.8 ± 0.5	$27.84 \pm 0.1\%$	$119.30 \pm 1.2\%$			
20.3 ± 0.5	$27.84 \pm 0.6\%$	$90.50 \pm 0.8\%$			
19.4 ± 0.5	$20.82 \pm 1.0\%$	$29.79 \pm 0.9\%$			
18.4 ± 0.5	$10.73 \pm 0.5\%$	$9.41 \pm 6.4\%$			
18.0 ± 0.5	$11.78 \pm 0.1\%$	$5.57 \pm 0.6\%$			
17.4 ± 0.6	$3.29 \pm 0.2\%$	$0.38 \pm 2.4\%$			
16.4 ± 0.6	$0.54 \pm 0.5\%$				
15.4 ± 0.6	$0.06 \pm 7.9\%$				

Energy in (MeV)	Cross section in milli barns	
	197-Tl	197-Hg (m)
52.0 ± 0.3	$1160.30 \pm 2.0\%$	$68.85 \pm 1.2\%$
50.7 ± 0.3	$1242.39 \pm 1.7\%$	$65.10 \pm 1.3\%$
49.4 ± 0.3	$1242.13 \pm 2.0\%$	$61.10 \pm 2.0\%$
48.0 ± 0.3	$1176.41 \pm 2.1\%$	$57.17 \pm 2.0\%$
46.6 ± 0.3	$1016.74 \pm 2.1\%$	$54.88 \pm 2.2\%$
45.1 ± 0.3	$861.25 \pm 2.3\%$	$51.08 \pm 2.2\%$
43.6 ± 0.3	$629.96 \pm 3.8\%$	$39.11 \pm 2.3\%$
42.1 ± 0.3	$386.70 \pm 6.6\%$	$25.53 \pm 4.4\%$
40.6 ± 0.3	$170.06 \pm 8.2\%$	$12.40 \pm 5.0\%$
38.8 ± 0.3		$2.93 \pm 3.0\%$
37.2 ± 0.4		$1.81 \pm 3.9\%$
35.5 ± 0.4		$0.85 \pm 6.8\%$

the reaction ^{181}Ta(α, n)^{184m,g}Re and ^{181}Ta(α, $2n$)^{183}Re are summarized and plotted as a function of α-particle bombarding energy. The experimental cross-sections are in millibarns and presented along with the percentage of statistical errors only. In table 3 and figure 2b the experimental results on the isomeric cross-section ratios for the isomer pair ^{184m,g}Re by the reaction ^{181}Ta(α, n)^{184m,g}Re are given as a function of α-particle bombarding energy. In table 4 the production cross-section as well as the isomeric cross-section ratios for the isomer pair ^{184m,g}Re by the reaction ^{185}Re($\alpha, \alpha n$)^{184m,g}Re are presented as a function of α-particle bombarding energy. Since the isomeric cross-section ratios are measured for the first time, no comparison could be made. In table 5 and figures 3a–e the total residual production cross-section in mb for the reactions figure (3a) ^{197}Au(α, n)^{200}Tl, figure (3b) ^{197}Au(α, $2n$)^{199}Tl, figure (3c) ^{197}Au($\alpha, 3n$)^{198m,g}Tl, figure (3d) ^{197}Au($\alpha, 4n$)^{197}Tl and figure (3e) ^{197}Au($\alpha, p3n$)^{197m}Hg are summarized and plotted as a function of α-particle bombarding energy. The absolute errors which is generally $\cong$ 8% consists of uncertainties due to target foil thickness ($\pm$2%), the beam

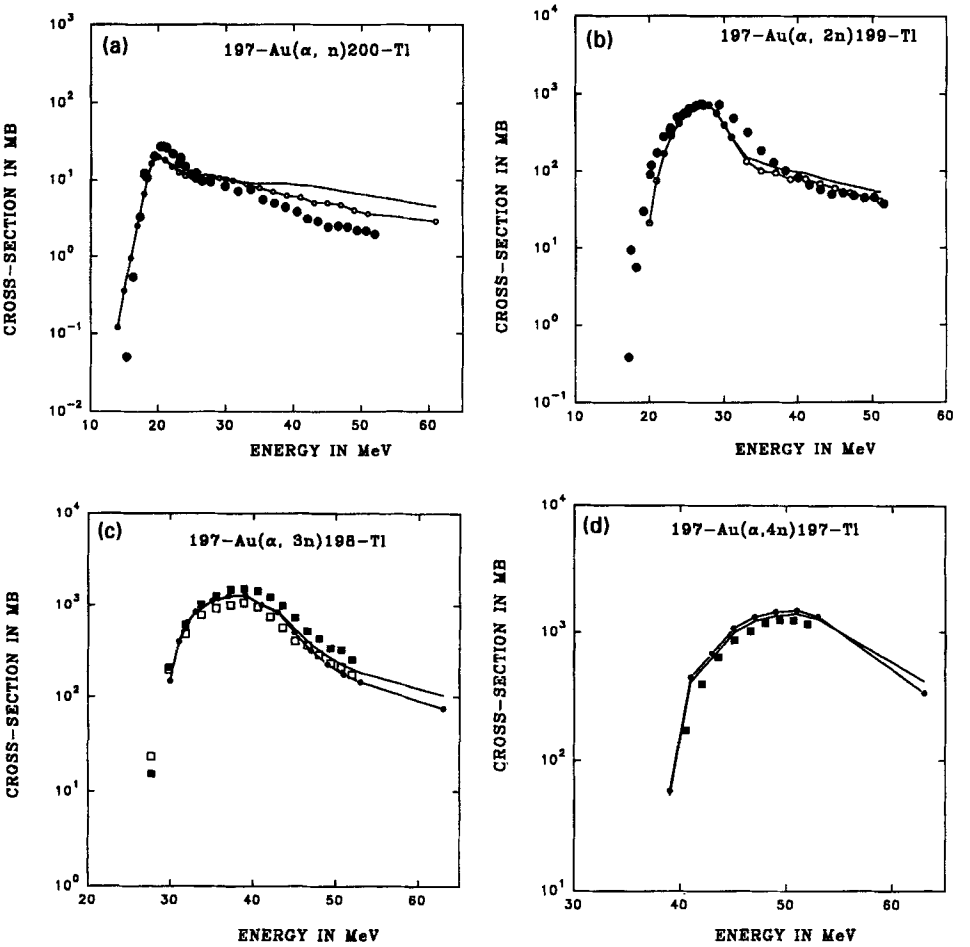

Figure 3(a–d).

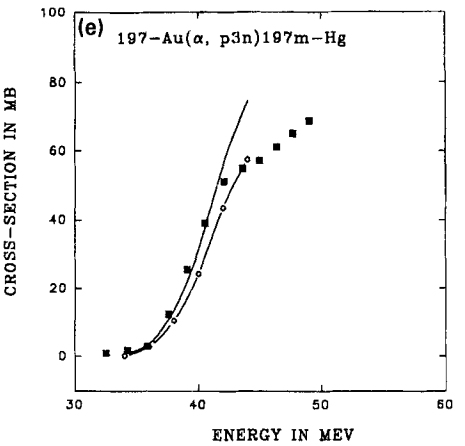

Figure 3a–e. The total residual production cross-section in mb for the reaction **(a)** ^{197}Au(α, n)^{200}Tl (•), **(b)** ^{197}Au(α, $2n$)^{199}Tl (•), **(c)** ^{197}Au(α, $3n$)^{198m,g}Tl (■ ⇒ m-state, □ ⇒ g-state), **(d)** ^{197}Au(α, $4n$)^{197}Tl (■) and **(e)** ^{197}Au(α, $p3n$)^{197m}Hg (■) for m-state) are plotted as a function of α-particle bombarding energy. Solid lines are the geometry dependent hybrid model and the –•– or –o– lines are the hybrid model fits using the code Alice/91 with $N_0 = 4, N_n = 2, N_p = 2$ and $N_h = 0$.

current integration (±2%), the detector efficiency (±5%) and the analysis of the γ-ray spectra (statistical uncertainty) generally ($\leq$ 2%). The uncertainties caused by the large size of the irradiation area and the non-uniformities of the target contribute about 5% to the average error of the cross-section. The uncertainty given for the energy values are those of target thickness only and beam energy resolution was $\cong$ ±200.0 keV only.

4. Comparison with theoretical predictions

We have investigated the nuclear mechanism of the nuclear reaction induced by α-particles using the computer codes Alice/91 [17] and Stapre [18]. The Alice/91 code [17] describes the process of equilibrium evaporation of particles and γ-rays in terms of the Weisskopf and Ewing model [24] and pre-equilibrium reaction mechanism according to the hybrid and geometry dependent hybrid model [1, 2]. Whereas in the Stapre code [18], the evaporation of particles and γ-rays are treated in the framework of the statistical model with consideration of angular momentum and parity using Hauser–Feshbach formalism [25]. For emission of the first particle pre-equilibrium decay is also taken into account. The pre-equilibrium emission of the particles was treated in the Stapre code [18] in the framework of exciton model [3]. The high energy parts of the excitation functions are dominated by pre-equilibrium reaction mechanism whereas the low energy parts are dominated by evaporation with its characteristic peak.

Most of the nuclear reaction models [1–6, 26, 27] to treat the pre-equilibrium phase of reactions leading to the formation of a compound nucleus are semi-classical in nature and have been used with considerable success in describing experimental data pertaining to the equilibration process, mainly the forward peaked hard component observed in the continuous spectra of light ejectiles and the high energy tails seen in the excitation

functions of activation cross-sections. However, most of these models employ one or both of the two basic concepts, the intranuclear cascade model [INC] [4, 5] and Griffin's statistical model of intermediate structure [3] (SMIS). The integral excitation functions of α-induced reactions have been discussed by several authors [7–10] considering models of the compound nucleus as well as pre-equilibrium reactions, as mentioned above. They conclude that the theory of pre-equilibrium reactions is helpful in explaining the mechanism of α-induced reactions. The hybrid model for pre-equilibrium reaction was proposed by Blann [1] which provides in some way a marriage between the simple SMIS model of Griffin [3] and the INC model using the more elaborate master equation approach due to Harp *et al* [4, 5]. However, there were some shortcomings in the hybrid model. It gives incorrect cross-sections and spectral distributions when applied to nucleon induced reactions at medium energies. Comparison with the INC model indicated that in the hybrid model, deficiencies resulted from the failure to take properly the enhanced emission from the nuclear surface. These deficiencies were partly rectified by reformulating the hybrid model as a sum of contributions, one term for each entrance channel impact parameter. In this way the diffuse surface properties sampled by the higher impact parameters were crudely incorporated into the precompound decay formalism in geometry dependent hybrid model (GDH) by Blann [2]. In the present work our excitation functions are calculated on the basis of hybrid model [1] and geometry dependent hybrid model [2] using the program Alice/91 [17] on the ND-500 and Super-32 computer at our centre.

The statistical part of the Alice/91 [17] can account for a large variety of reaction types. The evaporation of neutrons, protons and clusters such as deuteron and α-particles was considered [24]. The binding energies and Q-values used in the present code were based on experimental masses. The Alice/91 code [17] stores experimental masses in a data file. Whenever the nuclear masses are not tabulated, these were calculated from the Myers and Swiatecki mass formula [28], liquid drop masses with pairing. We have used the option in the default version of GDH whereby only the first collision is localized according to the impact parameter [29] with all the higher order precompound terms being treated by the hybrid model i.e. using nuclear densities averaged over the nucleus and independent of the impact parameter. This is reasonable because the excitons can sample nearly the entire nuclear volume after a single scattering since the mean free path (mfp) values are $\cong 4.74$ fm. The inverse cross-sections were calculated using the optical model subroutine of Alice/91 [17], where the optical model parameters were those of Becchetti and Greenlees [30]. The Fermi level density used is of the form

$$\rho(u) = (\sqrt{\pi}/12) \cdot (u - \delta)^{-5/4} \cdot a^{-1/4} \cdot \exp[2\sqrt{a(u - \delta)}],$$

where u is residual nucleus excitation, a is the level density parameter taken as $A/9\,\mathrm{MeV}^{-1}$ which is the default option of the code and $\delta = 11/\sqrt{A}\,\mathrm{MeV}$ the pairing energy shift, with either a backshifted or standard pairing shift option. We have used the standard option.

In the *a priori* formulation of the hybrid and geometry dependent hybrid model, the intra-nuclear transition rates are calculated either from the imaginary part of the optical model or from the free nucleon–nucleon scattering cross-section [31]. For particle energies exceeding 55 MeV the optical model parameters of Becchetti and Greenlees [30] used in the code are not applicable and thus at higher energies the calculation of the mean

free path for intra-nuclear transitions should be calculated from nucleon–nucleon scattering cross-sections. Since our bombarding energy range was below 55 MeV, we have used only optical model option for calculating the intra-nuclear transition rates.

The Stapre code [18] has been used to calculate the theoretical cross-sections and isomeric cross-section ratios for α-induced reactions taking into account up to six sequential evaporation of particles and γ-rays. Each evaporation step is treated within the framework of the statistical model with consideration of angular momentum and parity using Hauser–Feshbach formalism [25]. For the emission of the first particle pre-equilibrium decay is also taken into account. Direct interactions were not considered.

The parameters used in the code Stapre [18] were generally accepted ones. For calculation of the transmission coefficients of various particles for the code Stapre [18], the default global set of optical model parameters of Alice/91 code [17] was used. The transmission coefficients for γ-rays with transition energy ε_γ are expressed by the γ-ray strength function $f_{\mathrm{XL}}(\varepsilon_\gamma)$ for the multipole radiation of type XL. For the E1 strength function, the Brink–Axel [32] model with global parameters was used and for M1, E2, M2, E3 and M3 radiations, the Weisskopf model [33] was used. For energies, spins and parities of the discrete levels of the residual nuclei, the lowest 15–20 levels in [22] were used. The level density formalism of the back-shifted Fermi gas model expressed by Lang [34] was used for the continuum excitation energy region. The level density parameter $a = A/9$ was used for all nuclei, where A is the mass number of the nucleus. The spin distribution of the level density was characterized by the effective moment of inertia Θ_{eff} or better by its ratio to rigid body moment of inertia Θ_{rig} ($\eta = \Theta_{\mathrm{eff}}/\Theta_{\mathrm{rig}}$). Since isomeric cross-section ratios are expected to depend strongly on the effective moment of inertia, all the calculations were performed for $\eta = 0.5$ and $\eta = 1.0$.

In the Stapre code the pre-equilibrium emission of the particles were treated in the framework of exciton model [3] having the following ingredients. For the initial exciton configurations $(p_0 h_0)$ we used $(4, 0)$ for α-particles [17]. The transition rates were calculated by the formulae of Williams and Cline model [35]. The average residual two-body matrix element that appears in the transition rates λ_+, λ_0 and λ_- formulae as proposed by Kalbach–Cline [36] is expressed as

$$|M|^2 = FM \cdot A^{-3} \cdot E^{-1}, \tag{5}$$

where E is the excitation energy of the composite system. The quantity FM is a constant with the dimension of $(\mathrm{MeV})^3$ and generally treated as free parameter so as to get a good fit to the experimental data. The values used for the α-particle induced reactions were in the range $FM = 750$–$1000\,\mathrm{MeV}^3$.

In Alice [17] code, we have taken an initial exciton configuration $n_0 = 4$ $(n_n = 2, n_p = 2, n_h = 0)$ which is equivalent to a break-up of the incoming α-particle in the field of the nucleus and the nucleons occupying excited states above the Fermi energy gives a better description of the excitation function compared to other configurations for the α-particle bombarding energies up to 55.0 MeV. Therefore we have mostly used $n_0 = 4$ $(n_n = 2, n_p = 2, n_h = 0)$ configuration in most of our calculations. The total production cross-section in mb for the reactions in figure (1a) $^{193}\mathrm{Ir}(\alpha, 2n)^{195}\mathrm{Au}$ (■), figure (1b) $^{193}\mathrm{Ir}(\alpha, 3n)^{194}\mathrm{Au}$ (■), figure (1c) $^{(193),191}\mathrm{Ir}[\alpha, (4n)2n]^{193}\mathrm{Au}$ [(■), □] and figure (1d) $^{191}\mathrm{Ir}(\alpha, 3n)^{192}\mathrm{Au}$ (■) are plotted as a function of α-particle bombarding energy. The solid line is the geometry dependent hybrid model and the circle-line (–o–) is

the hybrid model fits using the code Alice/91 with $N_0 = 4, N_n = 2, N_p = 2$ and $N_h = 0$. In figure 2a the total residual production cross-section in mb for the reaction ^{181}Ta(α, n)^{184m,g}Re [symbols ■ ⇒ g, □ ⇒ m] are plotted as a function of α-particle bombarding energy. The solid line is the geometry dependent hybrid model fit using the code Alice/91 with $N_0 = 4, N_n = 2, N_p = 2$ and $N_h = 0$. The –•– and –○– lines are Stapre code calculations with $FM = 1000$ (MeV)^3 and $FM = 750$ (MeV)^3 respectively. In figure 2b and table 3 the isomeric cross-sections and their ratios are presented. The isomeric cross-section is practically constant at low bombarding energy with some tendency to increase at higher bombarding energy which means that at higher bombarding energy there is some tendency to populate the isomeric state preferentially. However, at very high excitation energy both the states are populated equally as seen in table 4 for the reactions ^{185}Re(α, αn)^{184m,g}Re. In figure 2c the total residual production cross-sections in mb for the reaction ^{181}Ta(α, $2n$)^{183}Re [• symbols] are plotted as a function of α-particle bombarding energy. The solid line is the geometry dependent hybrid model fit using the code Alice/91 with $N_0 = 4, N_n = 2, N_p = 2$ and $N_h = 0$. In figures 3a–e the total residual production cross-section in mb for the reactions figure (3a) ^{197}Au(α, n)^{200}Tl (•), figure (3b) ^{197}Au(α, $2n$)^{199}Tl (•), figure (3c) ^{197}Au(α, $3n$) ^{198g,m}Tl (■ ⇒ m-state and □ ⇒ g-state), figure (3d) ^{197}Au(α, $4n$)^{197}Tl (■) and figure (3e) ^{197}Au(α, $p3n$) ^{197m}Hg (■ ⇒ m-state) are plotted as a function of α-particle bombarding energy. The solid lines are the geometry dependent hybrid model and the circle-dashed lines (–○–) are hybrid model fits using the code Alice/91 with $N_0 = 4, N_n = 2, N_p = 2$ and $N_h = 0$.

In the energy range of the measurement both geometry dependent hybrid model and hybrid model fit all the excitation functions reasonably well taking limitations of the calculations into account. Considering the multitudes of uncertainties in pre-equilibrium calculations such as (i) range of equilibrium and pre-equilibrium reaction cross-section involved and (ii) in parameters such as inverse reaction cross-sections and level densities etc. Blann [31] considered that a result which is within a factor of two (i.e. 0.5 to 2.0) of the experimental result in absolute cross-section and which generally has the correct spectral shape and variation of yield with excitation energy is an encouraging result.

5. Conclusion

A consistent set of 18 excitation functions has been measured for α-induced reactions on Ir, Au, Ta and Re targerts. The reliability of the cross-section was checked by comparing our measurements on Au with previous measurements. As in the previous studies, we have also observed that the excitation functions of the reactions induced by α-particles show structure with an initial peak with a slowly decreasing high energy edge becoming a flat plateau. The lower energy peak corresponds to particle emission mainly by evaporation by completely equilibrated compound nucleus. Whereas the low cross-section higher energy flat plateau corresponds to pre-equilibrium emission of nucleons at initial stages of the nuclear reaction. Comparison of the experimental data with hybrid and GDH model calculation shows reasonably good agreement with GDH model fitting high energy shoulder better indicating geometry dependent (surface) effects are important at higher energies only. Therefore, we can conclude that the dominant mechanism for reaction induced by α-particle in the lower energy range of these measurements is fusion-

evaporation and only at the higher energy the pre-equilibrium emission becomes dominant.

Acknowledgements

The author thanks the operational staff of the cyclotron at VECC, Calcutta for running the cyclotron smoothly during the experiments, and Super-32 computer system of our centre for their assistance at various stages of calculations. He also thanks Dr. M Blann for supplying the Alice/91 code and Dr M Uhl for supplying the Stapre code.

References

[1] M Blann, *Phys. Rev. Lett.* **27**, 337 (1971)
[2] M Blann, *Phys. Rev. Lett.* **28**, 757 (1972)
[3] J J Griffin, *Phys. Rev. Lett.* **17**, 478 (1966)
[4] D G Harp, J M Miller and J B Berne, *Phys. Rev.* **165**, 1166 (1968)
[5] G D Harp and J M Miller, *Phys. Rev.* **C3**, 1847 (1971)
[6] M Blann, *Annu. Rev. Nucl. Sci.* **25**, 123 (1975)
[7] S A Hjorth, H Ryde, K A Hagemann, G Lovhoiden and J C Waddington *Nucl. Phys.* **A144**, 513 (1970)
[8] M Ismail and A S Divatia, *Pramana – J. Phys.* **30**, 193 (1988); B.A.R.C./1366 (1987)
M Ismail, *Pramana – J. Phys.* **32**, 605 (1989) and B.A.R.C/1407 (1988)
[9] M Ismail, *Phys. Rev.* **C41**, 87 (1990)
[10] J Ernst, R Ibowski, H Klampil, H Machner, T Mayer-Kuckuk and R Shanz, *Z. Phys.* **A306**, 301 (1982)
[11] C Kaltach, *Phys. Rev.* **C23**, 124 (1981)
[12] M L Goldberger, *Phys. Rev.* **74**, 1268 (1948)
[13] C J Mathews, B G Glagola, R A Moyle and V E Voila Jr., *Phys. Rev.* **C25**, 2181 (1982)
[14] I Dostrovsky, Z Frankel and G Friedlander, *Phys. Rev.* **116**, 683 (1959); **118**, 781 (1960); **118**, 791 (1960)
[15] F Puhlhofer, *Nucl. Phys.* **A280**, 267 (1977)
[16] Y Nagame, K Sueki, S Baba and H Nakahara *Phys. Rev.* **C41**, 889 (1990)
O A Capurro, M de la Vega Vedoya, C Wasilevsky and S J Nassiff, *J. Radioanalytical Nucl. Chem.* **89/2**, 519 (1985)
A Colboreanu, P Constanin and O Salageon, *Nucl. Phys.* **A383**, 251 (1982)
F Hermes, E W Jasper, H E Kurz, T Mayer-Kuchuk, P F A Goudsmit and H Arnold, *Nucl. Phys.* **A228**, 175 (1974)
F M Lanzafame and M Blann, *Nucl. Phys.* **A142**, 545 (1970)
[17] M Blann, Alice/85/300 *A Evaporation Code*, Lawrence Livermore National Laboratory, University of California Livermore UCID-20169 (1985)
M Blann and H K Vonach, *Phys. Rev.* **C28**, 1475 (1983)
[18] M Uhl and B Stromaier, *Computer code for particle-induced activation cross-section and related quantities*, Institut fur Radiumforchung und Kernphysik Report 76/01, 1976 and Addendum to this report. See also B Stromaier and M Uhl, International Atomic Energy Agency Report IAEA-SMR **43**, 313 (1980)
[19] C F Williamson, J P Boujot and J Picard, CEA-R 3042 (1966)
[20] J Kern, *Isabelle: A fortran non-linear least-square fit code for nuclear spectra* (University of Fribourg, Switzerland, 1970) (unpublished)
[21] J Kern, *Nucl. Inst. Method.* **79**, 233 (1970)
[22] C M Lederer and V S Shirley, *Table of Isotopes*, 7th edition (New York, John Wiley, 1978)
[23] A H Wapstra and G Audi, *Nucl. Phys.* **A432**, 1 (1985)

[24] V F Weisskopf and D H Ewing, *Phys. Rev.* **57**, 472 (1940)
[25] W Hauser and H Feshbach, *Phys. Rev.* **87**, 336 (1952)
[26] E Gadioli, E Gadioli-Erba, L Sajo-Bohus and G Tagliaferri, *Rev. Nuovo Cimento* **6**, 1 (1976)
[27] E Gadioli, E Gadioli-Erba and J J Hogan, *Phys. Rev.* **C16**, 1404 (1977)
[28] W D Mayers and W J Swiatecki, *Nucl. Phys.* **81**, 1 (1966)
W D Mayers and W J Swiatecki, *Ark. Fys.* **36**, 343 (1967)
[29] M Blann and H K Vonach, *Phys. Rev.* **C28**, 1475 (1983)
[30] F D Becchetti and F D Greenlees, *Phys. Rev.* **182**, 1190 (1969)
[31] M Blann, *Nucl. Phys.* **A213**, 570 (1973)
[32] G A Bartholomew *et al, Adv. Nucl. Phys.* (Plenum Press, N.Y., 1973) vol. 7, ch. 4
[33] J M Blatt and V F Weisskopf, *Theoretical Nuclear Physics* (Wiley, New York, 1952) p. 627
[34] D W Lang, *Nucl. Phys.* **77**, 545 (1966)
[35] C K Cline, *Nucl. Phys.* **A195**, 353 (1972)
[36] C Kalbach-Cline, *Nucl. Phys.* **A210**, 590 (1973)